*J. Fluid Mech.* (2005), *vol.* 526, *pp.* 277–302.  
DOI: 10.1017/S0022112004002915 Printed in the United Kingdom

# Particle pair separation in kinematic simulations

By D. J. THOMSON AND B. J. DEVENISH

The Met Office, FitzRoy Road, Exeter EX1 3PB, UK

(Received 5 August 2003 and in revised form 7 September 2004)

The separation of pairs of particles within turbulent flow fields constructed using the 'kinematic simulation' method is explored. A consequence of the way the flow is constructed is that, in contrast to real turbulence, there is no 'sweeping' of the smaller eddies by the larger eddies. The implications of this are investigated. A simple phenoenological argument is presented which predicts that the mean-square separation of the particle pairs should grow like $t^6$ in kinematic simulation. Simulations support this result for the case where a large mean velocity is added to the flow to exaggerate the sweeping problem and the inertial subrange is sufficiently long. In the absence of a large mean velocity, the situation is more complex with the simple phenomenological argument failing in the parts of the flow where the velocity is much smaller than the r.m.s. velocity and where there is no sweeping problem. The separation process then follows $t^6$ in the bulk of the flow but follows Richardson's classical $t^3$ law in regions where the velocity is much smaller than the r.m.s. velocity. Because of the way the size of these regions varies in time, the resulting mean-square separation grows like $t^{9/2}$. Both the $t^6$ and $t^{9/2}$ behaviours contrast with the classical Richardson $t^3$ law, which is believed to hold in reality, and raise questions about the applicability of the kinematic simulation approach to the separation of pairs in real turbulent flows.

## 1. Introduction

The way pairs of particles separate in turbulent flows is an important problem. This is because when material (or heat) is being dispersed by turbulence, the variability in the concentration of material and the spread of the material about its centre of mass are closely linked to the statistics of the motion of particle pairs (see e.g. Batchelor 1952; Durbin 1980; Thomson 1990). Several authors (e.g. Sabelfeld & Kurbanmuradov 1990; Fung *et al.* 1992; Elliott & Majda 1996; Flohr & Vassilicos 2000) have used the method of 'kinematic simulation' to simulate the separation of pairs of particles in inertial-subrange turbulence. In this method, a random velocity field with appropriate spectral properties is constructed by superimposing Fourier modes. Particle pairs are then tracked in the simulated flow. These simulations appear to have been successful in simulating the theoretically expected scaling law for particle separations, which takes the form

$$\langle r^2 \rangle = G_\Delta \varepsilon t^3$$

where $r$ is the particle separation after time $t$, $\varepsilon$ is the rate of dissipation of turbulent energy per unit mass, $G_\Delta$ is a constant, and $\langle - \rangle$ denotes an ensemble average. However, the values of $G_\Delta$ obtained are generally much smaller than those obtained in other models (e.g. Kraichnan 1966; Thomson 1990) and they are also small in comparison to the experimental value of Ott & Mann (2000), although it is not clear whether the Reynolds number of this experiment is high enough to be definitive.

In this paper we consider an aspect of kinematic simulation which is not reflected in real flows, namely the fact that there is no 'sweeping' (i.e. advection) of the smaller scale eddies by the larger scale flow. This is a consequence of the fact that the Fourier modes are chosen independently, with the small scales being uninfluenced in any way by the large scales. We show that, as a result, there is little *a priori* reason to expect the simulations to give $t^3$ behaviour, and we give a simple phenomenological argument which suggests that $\langle r^2 \rangle$ should, in kinematic simulations, grow like $t^6$. The essence of the argument is that the large scales of the kinematic simulation, which sweep the particle pairs but not the inertial-subrange eddies, can influence the rate of separation, and this large-scale influence can upset the inertial-subrange scaling behaviour. In this connection we note that Kurbanmuradov, Sabelfeld & Koluhin (1997) carried out kinematic simulations of pair separation in which they found an exponent larger than 3 (although not as large as 6). They found that their simulations could be fitted by an expression of the form $\langle r^2 \rangle \sim G_\Delta \varepsilon t^3 ((\varepsilon t^3)^{1/2}/L)^\gamma$ where $L$ is the integral length scale, consistent with the idea of an influence from the large scales.

Some simulations are conducted to investigate this further. The behaviour of these simulations is easiest to understand for the case where a large mean flow is added in order to exaggerate the 'sweeping' problem. For this case, the simulations confirm that the asymptotic behaviour for a long inertial subrange is indeed $t^6$. When there is no mean flow, the situation is more complex. For this case the results are significantly influenced by the regions where the velocity is very small, i.e. regions in which there is no sweeping problem. A consequence of this is that the simple phenomenological argument which predicts $t^6$ fails, but a more complicated argument leads to the prediction that $\langle r^2 \rangle$ grows in proportion to $t^{9/2}$. This is confirmed by the simulations.

## 2. A phenomenological argument

Consider the time scale $\tau(r)$ on which the relative velocity of particles of separation $r$ changes. Provided this time scale is not large, the use of a separation-dependent eddy diffusivity $K(\boldsymbol{r})$ should give a reasonable estimate of the rate of separation of particle pairs. Of course an eddy diffusivity will give accurate results only if $\tau$ is small compared to the travel time $t$. However, provided $\tau$ is not large compared to $t$, we expect an eddy diffusion assumption to at least provide the correct scaling. For separations in the inertial subrange, $K(r) \sim (\varepsilon r)^{2/3} \tau(r)$ (assuming a mean-square velocity difference over a distance $r$ of order $(\varepsilon r)^{2/3}$, as is appropriate in the inertial subrange). This leads to

$$\frac{\mathrm{d}\langle r^2 \rangle}{\mathrm{d}t} \sim K\left(\langle r^2 \rangle^{1/2}\right) \sim \varepsilon^{2/3} \langle r^2 \rangle^{1/3} \tau\left(\langle r^2 \rangle^{1/2}\right). \tag{1}$$

Here we have evaluated $K$ at a typical value of $r$, namely $\langle r^2 \rangle^{1/2}$. This will give the right scaling behaviour when the diffusion equation has a similarity solution.

In reality (ignoring intermittency corrections) we expect the inertial subrange to depend only on $\varepsilon$ and hence the time scale $\tau(r)$ to be proportional to $r^{2/3}/\varepsilon^{1/3}$. This gives Richardson's (1926) classical scaling with $K(r) \sim \varepsilon^{1/3} r^{4/3}$ and, once the initial separation is forgotten, equation (1) yields $\langle r^2 \rangle \sim \varepsilon t^3$ (see e.g. Monin & Yaglom 1975, p. 574). One can also consider white-noise velocity fields where we obtain $K \sim r^{2/3}$ and $\langle r^2 \rangle \sim t^{3/2}$ (at least if we take the white noise limit in such a way that the correlation time is independent of separation and the velocity structure function remains proportional to $r^{2/3}$). This white noise case is one where exact results can be obtained (see e.g. Kraichnan 1968, 1994; Eyink & Xin 2000). It is of course more

physically appropriate to take the white noise limit in such a way that $K$ retains the Richardson scaling and varies like $r^{4/3}$. In this case we rigorously obtain $\langle r^2 \rangle \sim t^3$.

In kinematic simulations the time scale $\tau$ is likely to be different from either of the above cases. This is because the small eddies are not swept by the large eddies, while the particles are so swept. This means that the particles are swept rapidly through the small eddies by the large eddies. If we assume the separation process is dominated by eddies of similar size to the particle separation $r$, then we expect $\tau$ to be of order the time taken to sweep the particles through an eddy of size $r$, i.e. we expect $\tau \sim r/U$ where $U$ is the characteristic large-scale sweeping velocity. $U$ might be the r.m.s. turbulent velocity if there is no mean flow, or the mean velocity if the turbulence is not advected with the mean flow (as in the case studied by Elliott & Majda (1996) and in some of our simulations below). This leads to the prediction $K(r) \sim \varepsilon^{2/3} r^{5/3}/U$ and

$$\langle r^2 \rangle \sim \frac{\varepsilon^4}{U^6} t^6.$$

In fact, for small $r$, the sweeping time scale $r/U$ is much smaller than the classical inertial-subrange time scale $r^{2/3}/\varepsilon^{1/3}$ and so we should perhaps have more confidence in the relevance of these eddy diffusivity arguments for kinematic simulation than for real turbulence. On the other hand, the argument ignores variations in the sweeping velocity, and these variations could perhaps cause the argument to fail. These issues are investigated below.

## 3. Simulations

A number of simulations were conducted to test the above ideas. In each simulation, the kinematic simulation approach was used to generate an ensemble of random isotropic incompressible three-dimensional velocity fields. The velocity at position $\boldsymbol{x}$ at time $t$ is given by

$$\boldsymbol{u}(\boldsymbol{x}, t) = \sum_{n=1}^{N} \boldsymbol{A}_n \cos(\boldsymbol{k}_n \cdot \boldsymbol{x} + \omega_n t) + \boldsymbol{B}_n \sin(\boldsymbol{k}_n \cdot \boldsymbol{x} + \omega_n t) \tag{2}$$

where $N$ is the number of modes, $\boldsymbol{k}_n$ and $\omega_n$ are the wavenumber vector and frequency of the $n$th mode, and $\boldsymbol{A}_n$ and $\boldsymbol{B}_n$ are the mode amplitudes. The wavenumber vector $\boldsymbol{k}_n$ is chosen as $k_n \hat{\boldsymbol{k}}_n$ where $\hat{\boldsymbol{k}}_n$ is a unit vector in a random direction (i.e. with the end point of the vector uniformly distributed over the unit sphere) and $k_n$ is chosen as described below. The amplitudes $\boldsymbol{A}_n$ and $\boldsymbol{B}_n$ are chosen to have random directions perpendicular to $\hat{\boldsymbol{k}}_n$ (in practice these directions are generated by taking unit vectors of random direction and taking the vector product with $\hat{\boldsymbol{k}}_n$) and magnitudes $A_n$ and $B_n$ given by

$$A_n^2 = B_n^2 = 2E(k_n)\Delta k_n.$$

Here $E(k)$ is a prescribed energy spectrum

$$E(k) = \begin{cases} \alpha \varepsilon^{2/3} k^{-5/3} & \text{for } 2\pi/L \leqslant k \leqslant 2\pi/\eta \\ 0 & \text{otherwise} \end{cases}$$

where $k$ is the wavenumber, $\varepsilon$ is the notional energy dissipation rate (there is of course no actual dissipation in kinematic simulation), $L$ and $\eta$ are proportional to the integral length scale and the Kolmogorov dissipation length scale respectively, and $\alpha$

is the Kolmogorov constant. The energy spectrum is defined here so that

$$\int_0^\infty E(k)\,\mathrm{d}k$$

is the turbulent energy per unit mass. The interval $\Delta k_n$ is defined by

$$\Delta k_n = \begin{cases} (k_2 - k_1)/2 & \text{for } n = 1 \\ (k_{n+1} - k_{n-1})/2 & \text{for } 2 \leqslant n \leqslant N-1 \\ (k_N - k_{N-1})/2 & \text{for } n = N, \end{cases}$$

where $k_1 = k_L = 2\pi/L$ and $k_N = k_\eta = 2\pi/\eta$. The wavenumbers are discretized according to the geometric sequence

$$k_n = k_L a^{n-1}, \quad n = 1, \ldots, N,$$

where $a = (L/\eta)^{1/(N-1)}$. The above approach to generating the velocity field closely follows e.g. Fung & Vassilicos (1998) and Malik & Vassilicos (1999).

As $N$ increases, the statistics of the velocity field become Gaussian and independent of the choice of distribution of the wavenumbers, at least provided that the maximum of the $\Delta k_n$ becomes small, a condition which ensures that the contribution to the energy from any one mode becomes small. (In this limit, the contribution to $\boldsymbol{u}$ from any given small region of $\boldsymbol{k}$-space is the sum of many modes which are independent and close to being identically distributed. Gaussianity then follows from application of the central limit theorem together with a weak compactness argument along the lines given by Kurbanmuradov (1995) – see Thomson & Devenish (2003) for details.) However, despite this asymptotic lack of dependence on the choice of distribution of the wavenumbers, the use of a geometric sequence for the $k_n$ is important to ensure that a reasonable number of modes are present in any wavenumber range $(k, 2k)$ while keeping the computational cost from becoming excessive.

The frequency $\omega_n$ in (2) determines the unsteadiness associated with the $n$th mode. The majority of our simulations involve a frozen velocity field with $\omega_n = 0$. However, we also conduct some studies with $\omega_n$ proportional to the eddy turnover time of the $n$th mode, that is,

$$\omega_n = \lambda\sqrt{k_n^3 E(k_n)}, \tag{3}$$

where $\lambda$ is a dimensionless constant of order one. In reality we expect the phase of each mode to change with a frequency associated with the sweeping of the mode by the large scales and/or mean flow. This leads to an alternative possible scaling for $\omega_n$ with $\omega_n$ of order $k_n U$ (see e.g. Kraichnan 1959; Tennekes 1975; Fung *et al.* 1992; Fung & Vassilicos 1998). However, this alternative seems inappropriate in a model where such sweeping does not occur and we have not considered it further here.

In some of our simulations the mean flow $\overline{\boldsymbol{U}}$ is non-zero, and then $\overline{\boldsymbol{U}} = (\overline{U}, 0, 0)$ is simply added to the right-hand side of equation (2). This exaggerates the sweeping problem because the eddy structures are not advected with the mean flow. When $\overline{U}$ is much greater than the r.m.s. turbulent velocity fluctuations, the velocity with which the particle pairs are advected through the eddies is dominated by $\overline{U}$ and so, to leading order, is uniform throughout the flow. As a result it seems likely that the fluctuations in the sweeping velocity can be neglected, leading to a situation which is easier to understand and analyse than cases with small or zero $\overline{U}$.

With the above form for $E(k)$ we have $\sigma_u^2 = \alpha(\varepsilon/2\pi)^{2/3}(L^{2/3} - \eta^{2/3})$ where $\sigma_u$ is the r.m.s. value of any one component of the velocity fluctuations. In all our simulations we have $\eta \ll L$ and so $\sigma_u^2 = \alpha(\varepsilon/2\pi)^{2/3} L^{2/3}$ to quite high accuracy. We choose $\sigma_u = L = 1$

for all our simulations, but present results in non-dimensional form so that this is transparent to the reader. However this choice, and the desire to avoid assuming a particular value for $\alpha$, means that it is often more convenient to use $\sigma_u$ and $L$ for non-dimensionalization than $\varepsilon$. Hence in particular we introduce $\epsilon = \sigma_u^3/L$ – a quantity of order $\varepsilon$ and numerically equal to 1 – and use this instead of $\varepsilon$ where this is convenient.

Particle pairs were released with separation $r_0$ and tracked through the flow. The initial positions of the particle pairs were chosen by placing one particle from each pair on a uniform cubic lattice of side $L$ and placing the other particle at a distance $r_0$ in a random direction. The advection of the particle pair was calculated using the forward Euler method. We expect the separation process to be dominated by eddies whose size is of order the particle separation $r$ when $r$ lies in the inertial subrange, and more generally by eddies of size $\min(\max(r, \eta), L)$. For most of the simulations, an adaptive time-step was used which is given by

$$\Delta t = \min\left( C_1 \frac{\min(r, L)}{\max(\overline{U}, \sigma_u)}, C_2 \frac{[\min(r, L)]^{2/3}}{\lambda \epsilon^{1/3}} \right) \tag{4}$$

where $C_1$ and $C_2$ are constants. For small values of the constants this should ensure that the time-step is small enough to resolve the changes in particle velocity due to (i) the sweeping of particles through the eddies that dominate the separation process, and (ii) the temporal change of such eddies caused by $\lambda$. Sensitivity tests (presented below) suggest that the choices $C_1 = 0.1$ and $C_2 = 0.01$ are adequate and these values are used except where indicated.

Our main interest is in the behaviour when the separation is dominated by inertial–convective processes. For such a regime to exist in reality we require $\eta \ll L$ (so that there is a long inertial subrange in the velocity field) and $r_0 \ll L$ (so that the separation process is not dominated by the eddies with size of order $L$). We also require $r_0 \not\ll \eta$; this is because $r_0 \ll \eta$ can lead to a long-lasting regime where the separation is dominated by viscous–convective processes. ($r_0 \ll \eta$ does not necessarily exclude the possibility of a regime dominated by inertial–convective processes occurring after the viscous–convective regime provided $\eta/L$ is small enough, but we will not consider this possibility here.) In all our simulations the parameters will be chosen to be consistent with these conditions so as to give a chance of inertial–convective behaviour occurring, although it is not clear *a priori* how small $\eta/L$ and $r_0/L$ need to be to see the true asymptotic behaviour.

As noted above, the situation with a large mean velocity should be simpler to understand because the (fractional) variations in the sweeping velocity are small and can, we hope, be neglected. As a result we present this situation first in § 3.1. The more complicated situation with zero mean flow is presented in § 3.2. The simulations were performed on an NEC SX-6 supercomputer using 64-bit precision (32-bit precision is incapable of representing the problem at all accurately, for example in representing correctly the small change over a time-step in the separation of close particles, when the particle coordinates are not small).

### 3.1. *Large mean velocity*

Figure 1 shows the evolution of the mean-square separation $\langle r^2 \rangle$ as computed using the kinematic simulation technique for the case of a strong mean flow with $\overline{U} = 10\sigma_u$. A range of initial separations $r_0$ is used with two values of $\eta/L$, namely

$$r_0/L = 10^{-6}, 10^{-5}, 10^{-4} \text{ and } 10^{-3} \text{ with } \eta/L = 10^{-6} \text{ and 1200 modes}$$

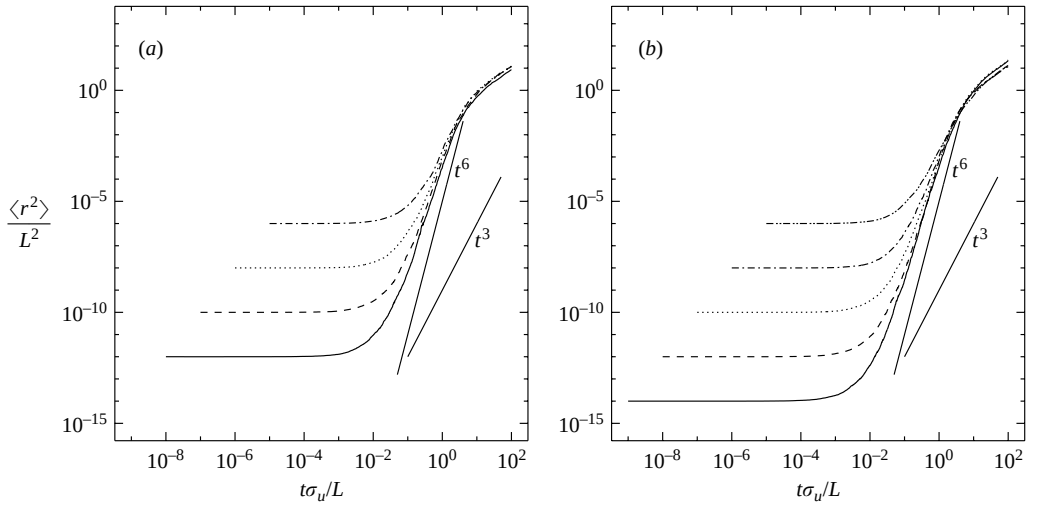


FIGURE 1. The evolution of $\langle r^2\rangle$ for $\overline{U}=10\sigma_u$, $\lambda=0$, 125 particle pairs per realization and 5 realizations of the flow in each simulation: (*a*) $r_0/L=10^{-6}$, $10^{-5}$, $10^{-4}$ and $10^{-3}$ (bottom to top) with $\eta/L=10^{-6}$ and $N=1200$; (*b*) $r_0/L=10^{-7}$, $10^{-6}$, $10^{-5}$, $10^{-4}$ and $10^{-3}$ with $\eta/L=10^{-8}$ and $N=1600$. The straight lines are proportional to $t^3$ and $t^6$.

and

$$r_0/L = 10^{-7}, 10^{-6}, 10^{-5}, 10^{-4} \text{ and } 10^{-3} \text{ with } \eta/L = 10^{-8} \text{ and } 1600 \text{ modes.}$$

These simulations are steady flows (i.e. $\lambda=0$) with 125 particle pairs per realization and five realizations of the flow in each simulation. If the separation $\boldsymbol{r}$ were Gaussian and the pairs independent, this number of pairs would lead to errors in $\langle r^2\rangle$ of order 3%. Here we expect somewhat larger errors because $\boldsymbol{r}$ is likely to be more peaked than Gaussian and because the small number of flow fields means that the pairs are not completely independent. Nonetheless we expect this to be accurate enough for our purposes, which involve looking at the evolution of $\langle r^2\rangle$ over many orders of magnitude. For confirmation of this see figure 8 below which shows small differences (relative to the range over which $\langle r^2\rangle$ varies) between independent realizations of the flow.

Examination of figure 1 shows that $\langle r^2\rangle \approx r_0^2$ at small times but then, at least for the smaller values of $r_0$, grows approximately like $t^6$. At large times the particle separation becomes large and the particles move approximately independently and diffusively (following the ideas of Taylor 1921), and so $\langle r^2\rangle$ grows linearly with $t$. The results are consistent with the expectation that, for small $r_0/L$ and $\eta/L$ (with $r_0 \ll \eta$), the values of $r_0$ and $\eta$ are forgotten at large times and that this happens long before the linear regime is reached. Neither the $t^6$ regime nor the independence from $r_0$ are satisfied to great accuracy. However this is perhaps to be expected. With a $t^6$ growth rate and $\eta/L=10^{-6}$, $\langle r^2\rangle$ can increase from $\eta^2$ to $L^2$ while time increases by only a factor of 100, which is quite a small ratio of times to expect the true asymptotic power-law regime to be established accurately. It seems likely that in real turbulence the $t^3$ regime could be established at much smaller values of $L/r_0$ and $L/\eta$ than are needed in kinematic simulation to get $t^6$. Figure 2 shows the evolution of $\langle r^2\rangle/t^6$ for the $\eta/L=10^{-8}$ simulations. It is clear that, as $r_0/L$ decreases, $\langle r^2\rangle$ comes closer to showing $t^6$ behaviour at intermediate travel times. It seems plausible to assume that

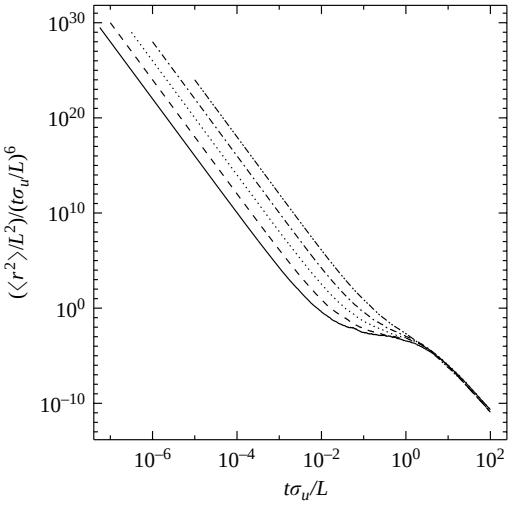


FIGURE 2. The evolution of $\langle r^2\rangle/t^6$ for the simulations shown in figure 1(*b*).

the $t^6$ region will become more convincing and longer with decreasing $r_0/L$ (and with $\eta/L$ decreasing to ensure $r_0 \ll \eta$). The computational cost however prevents us from exploring this here.

We will now consider the stages in the evolution of $\langle r^2\rangle$ in more detail. For $\eta \ll r_0 \ll L$, we expect to see four ranges in the evolution of the mean-square separation. (Note that we have adopted a slightly stronger condition than the conditions $r_0 \ll L$ and $r_0 \ll \eta$ considered above; this is necessary to obtain the first two ranges). At small times particles move in approximately straight lines and we have $\langle r^2\rangle \approx r_0^2 + \tilde{D}_{ii}(r_0)t^2$ where $D_{ij}(\boldsymbol{r})$ is the velocity structure function and $\tilde{D}_{ij}(r_0)$ denotes $D_{ij}(\boldsymbol{r}_0)$ averaged over the random direction of $\boldsymbol{r}_0$. (Of course $D_{ii}(\boldsymbol{r}_0)$ does not depend on the direction of $\boldsymbol{r}_0$, but this tilde notation will be useful below in connection with the diffusivity). In the inertial subrange, $D_{ij}(\boldsymbol{r})$ is given by

$$D_{ij}(\boldsymbol{r}) = C\varepsilon^{2/3}r^{2/3}\left(\frac{4}{3}\delta_{ij} - \frac{1}{3}\frac{r_i r_j}{r^2}\right) \tag{5}$$

with $C = 27\Gamma(1/3)\alpha/55$ (see Monin & Yaglom 1975, p. 355). This regime should persist to times of order the relative velocity Lagrangian correlation time scale $\tau(r_0)$ for particles of separation $r_0$, which is of order $r_0/\overline{U}$ (because of the sweeping effect discussed in § 2). Then we expect a regime dominated by an approximately constant diffusivity $\tilde{K}_{ij}(r_0) \sim \varepsilon^{2/3}r_0^{5/3}/\overline{U}$, with $\langle r^2\rangle \approx r_0^2 + 2\tilde{K}_{ii}(r_0)t$. Here we have acknowledged in the notation that $K$ will be a tensor, an issue which we glossed over in § 2. Also, unlike $D_{ii}$ above, $K_{ii}(\boldsymbol{r}_0)$ may depend on the direction of $\boldsymbol{r}_0$ through the angle between $\boldsymbol{r}_0$ and the mean velocity, and in fact we will see below that it does so depend. This regime will persist until the 'take-off time' $t_{to}$ at which $\langle r^2\rangle - r_0^2$ becomes comparable to $r_0^2$ itself, with $t_{to}$ being of order $r_0^{1/3}\overline{U}/\varepsilon^{2/3}$. Beyond this time, the particles have a range of values of $r$ and the variation of $K$ with $r$ comes into play. Here we expect the $\langle r^2\rangle \sim \varepsilon^4 t^6/\overline{U}^6$ regime to develop and persist until $\langle r^2\rangle$ becomes of order $L^2$ which happens at $t \sim L^{1/3}\overline{U}/\varepsilon^{2/3} \sim L\overline{U}/\sigma_u^2$. Finally we expect the large-time diffusive regime with $\langle r^2\rangle \sim \sigma_u^2\tau(L)t \sim \sigma_u^2 Lt/\overline{U}$. It can be easily checked that these regimes match appropriately.

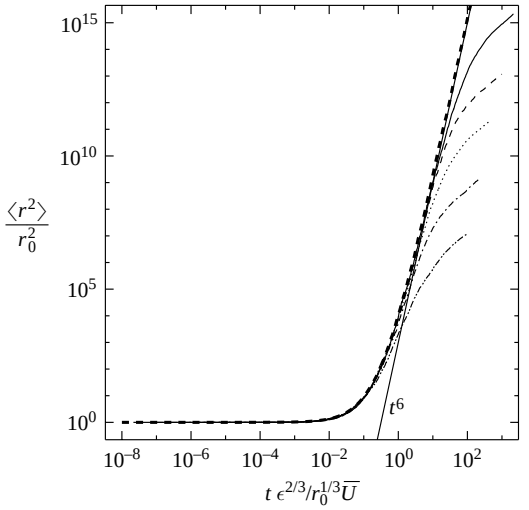


FIGURE 3. The evolution of $\langle r^2\rangle$ for the simulations shown in figure 1($b$) and for the eddy-diffusivity model (shown as short thick dashes). The straight line is proportional to $t^6$.

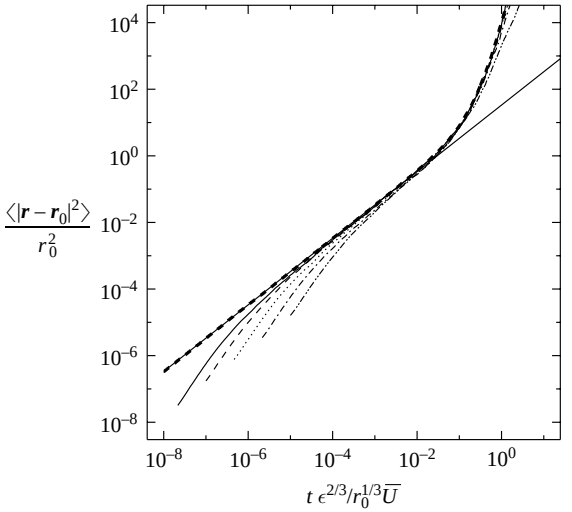


FIGURE 4. The evolution of $\langle|\boldsymbol{r}-\boldsymbol{r}_0|^2\rangle$ for the simulations shown in figure 1($b$) and for the eddy-diffusivity model (shown as short thick dashes). The straight line is $\langle|\boldsymbol{r}-\boldsymbol{r}_0|^2\rangle = 2\tilde{K}_{ii}(r_0)t$.

In the second and third of these regimes and in the transition between them, the behaviour is controlled by an eddy diffusivity which varies as $\varepsilon^{2/3}r^{5/3}/\overline{U}$ as discussed in § 2 above. Here we expect the evolution of $\langle r^2\rangle$ to be universal when non-dimensionalized using $r_0$ and $\epsilon^{2/3}/\overline{U}$, i.e. when plotted as $\langle r^2\rangle/r_0^2$ against $t\epsilon^{2/3}/r_0^{1/3}\overline{U}$, the latter being of order $t/t_{to}$. We also expect $\langle r^2\rangle$ (although not $\langle r^2\rangle - r_0^2$) to be universal in this scaling at smaller times (where, to leading order, $\langle r^2\rangle \approx r_0^2$). Figure 3 shows that results are indeed universal until the transition to the large-time linear-growth regime, although, as noted above, this happens too soon to see a really convincing third regime proportional to $t^6$. To explore the first two regimes in more detail we have plotted $\langle|\boldsymbol{r}-\boldsymbol{r}_0|^2\rangle/r_0^2$ against $t\epsilon^{2/3}/r_0^{1/3}\overline{U}$ in figure 4. Note that, because

$\langle \boldsymbol{r} \rangle$ equals $\boldsymbol{r}_0$ (at least in the limit of a large number of particles), $\langle |\boldsymbol{r} - \boldsymbol{r}_0|^2 \rangle$ is equal to $\langle r^2 \rangle - r_0^2$ . The results confirm the universality of the second regime and the start of the transition to the third (although, for the smallest value of $L/r_0$, the effect of $L$ is beginning to be significant at the largest times plotted), and also confirm that the first regime is not universal when plotted in this way. The collapse in figures 3 and 4 extends to the simulations with $\eta/L = 10^{-6}$ (not shown). It is of interest that this includes the case with $r_0 = \eta$, so this appears in practice to satisfy the condition $r_0 \gg \eta$ to sufficient accuracy!

We have already defined $\tau$ as a function of $r$; $t_{to}$ can also be regarded as a function of $r$ if defined as the time for which particle pairs at separation $r$ do not change their separation by more than a factor of order unity. In the inertial subrange we have that $t_{to}(r)$ is of order $r^{1/3}\overline{U}/\epsilon^{2/3}$. In the classical Richardson scaling, the two time scales $\tau$ and $t_{to}$ are the same, whereas in kinematic simulation with $\overline{U} \gg \sigma_u$ we have $t_{to}(r) \gg \tau(r)$. As a result the pair separation process reaches its diffusive limit long before the inhomogeneity of the relative dispersion process becomes significant. This means that (i) the relative-velocity Lagrangian correlation integral time scale can be defined precisely, (ii) the eddy-diffusivity assumption for the separation process should be accurate, and (iii) we can also make a quantitative calculation of the value of $K_{ij}$. This is true even outside the inertial subrange, but for simplicity we will only consider the inertial subrange case here. The eddy diffusivity for the particle pair separation may be calculated as

$$K_{ij}(\boldsymbol{r}) = \frac{1}{2}\int_{-\infty}^{\infty} \langle \Delta u_i(t) \Delta u_j(t+t') \rangle \, \mathrm{d}t' \tag{6}$$

where the integrand is the Lagrangian correlation of the relative velocities at time $t$ and time $t+t'$ for particles with separation $\boldsymbol{r}$. This is analogous to Taylor's theory for one-particle dispersion (see e.g. Pasquill & Smith 1983, p. 115). The separation changes little over the time $\tau(r)$ that $\Delta u_i$ and $\Delta u_j$ are correlated and the change in the position of the particles is dominated by the mean velocity $\overline{\boldsymbol{U}}$. Thus, for a particle at position $\boldsymbol{x}$ at time $t$, the position at time $t+t'$ is $\boldsymbol{x} + \overline{\boldsymbol{U}}t'$. Hence

$$\begin{aligned} \langle \Delta u_i(t) \Delta u_j(t+t') \rangle &= \langle (u_i(\boldsymbol{x}) - u_i(\boldsymbol{x}+\boldsymbol{r}))(u_j(\boldsymbol{x}+\overline{\boldsymbol{U}}t') - u_j(\boldsymbol{x}+\boldsymbol{r}+\overline{\boldsymbol{U}}t')) \rangle \\ &= \tfrac{1}{2}[D_{ij}(\overline{\boldsymbol{U}}t' - \boldsymbol{r}) + D_{ij}(\overline{\boldsymbol{U}}t' + \boldsymbol{r}) - 2D_{ij}(\overline{\boldsymbol{U}}t')] \end{aligned} \tag{7}$$

where for the last step we have used a standard result on structure functions given by Monin & Yaglom (1975, p. 102). In the inertial subrange $D_{ij}$ is given by (5) and the diffusivity can be calculated to be

$$K_{ij}(\boldsymbol{r}) = \frac{\sqrt{\pi}}{6}\frac{\Gamma(1/6)}{\Gamma(2/3)}\frac{C\varepsilon^{2/3}r^{5/3}}{\overline{U}}(1-\beta^2)^{5/6}\left[\frac{8}{5}\delta_{ij} + \frac{3}{5}\hat{U}_i\hat{U}_j - \frac{(\hat{r}_i - \beta\hat{U}_i)(\hat{r}_j - \beta\hat{U}_j)}{1-\beta^2}\right] \tag{8}$$

where $\hat{\boldsymbol{r}}$ and $\hat{\boldsymbol{U}}$ are unit vectors in the direction of $\boldsymbol{r}$ and $\overline{\boldsymbol{U}}$ and $\beta$ equals $\hat{\boldsymbol{r}} \cdot \hat{\boldsymbol{U}}$. Details of this calculation are given in Thomson & Devenish (2003). We note that $K_{ij}$ is divergence free (i.e. $\partial K_{ij}/\partial r_j = 0$), a property which it inherits from $D_{ij}$. We also note that $K_{ij}$ is independent of the component of $\boldsymbol{r}$ in the direction of the mean flow (that is, for our choice $\overline{\boldsymbol{U}} = (\overline{U}, 0, 0)$ of mean flow, $K_{ij}$ depends on $\boldsymbol{r}$ only through $r_2$ and $r_3$) and is zero when $\boldsymbol{r}$ is aligned with $\overline{\boldsymbol{U}}$. This is because, to the extent that the above approximations are valid, the effect of displacing a particle in the direction of the mean flow is simply to alter the time at which the particle encounters the various eddies.

Alongside the kinematic simulation results in figures 3 and 4, we have also plotted the results obtained from the diffusion equation with $K_{ij}$ given by (8). These results

were obtained via the equivalent stochastic differential equation

$$\mathrm{d}r_i = b_{ij}\,\mathrm{d}\xi_j \tag{9}$$

where $\xi_j$ is a Wiener process and $b_{ij}$ satisfies $2K_{ij} = b_{ik}b_{jk}$. The matrix $\boldsymbol{b}$ was calculated by Cholesky decomposition. Equation (9) was simulated by a random walk technique using a forward step with an adaptive time-step based on $t_{to}(r)$ and given by

$$\Delta t = C_3 \frac{r^{1/3}\overline{U}}{\epsilon^{2/3}}$$

(although in fact, because we want to plot output at times smaller than $t_{to}(r_0)$, we also limit the time-step by the first required output time and, after the first step, we ensure it does not exceed $0.1t$ so that we can linearly interpolate the position to the desired output time without much loss of accuracy). Sensitivity tests (presented below) suggest that the choice $C_3 = 10^{-3}$ is adequate and this value is used except where indicated. The simulation was run with the size of the initial separation fixed but with the direction random, the initial separation vector $\boldsymbol{r}_0$ being distributed uniformly over a sphere. 5000 particle pairs were followed. Figure 3 shows very good agreement between the kinematic simulation and the eddy-diffusivity model until the transition to the large-time linear-growth regime. The eddy diffusivity model assumes an infinite inertial subrange and so is of course not expected to capture the large-time behaviour. Figure 4 also shows good agreement between the kinematic simulation and the eddy diffusivity model except at small times where the eddy diffusion approximation is not valid and, for $L/r_0 = 10^3$, at the largest times plotted where the effect of $L$ is beginning to be significant. In figure 4 we have also plotted the line

$$\langle |\boldsymbol{r} - \boldsymbol{r}_0|^2 \rangle = 2\tilde{K}_{ii}(r_0)t = \frac{27}{40}\pi(2\pi)^{2/3}\frac{\Gamma(1/6)\Gamma(5/6)}{\Gamma(2/3)}\frac{\epsilon^{2/3}r_0^{5/3}t}{\overline{U}}. \tag{10}$$

The simulation results give support to this being the correct asymptote for the regime $\tau(r_0) \ll t \ll t_{to}(r_0)$.

A number of further kinematic simulations were conducted in order to investigate the sensitivity to the choice of time-step, to the number of modes used, and to $\lambda$. These simulations are all based on the case with $r_0/L = 10^{-5}$ and $\eta/L = 10^{-6}$ shown above (this case will be referred to as the 'base case'), but with various alterations as described below. The base case is not our 'best' simulation in that others involve a wider range of scales; however it is sufficiently computationally cheap to allow a wide range of sensitivity tests.

To test whether our time-step is small enough, we compare the base case with two other simulations, one with a fixed time-step of $0.1\eta/\overline{U}$ and one with an adaptive time-step given by (4) with $C_1 = 0.01$ (i.e. reduced by a factor of 10 relative to the base case). In the simulation with $\Delta t = 0.1\eta/\overline{U}$, the particles should follow even the smallest eddies, although these eddies are expected to have little effect on the separation process when $r \gg \eta$. Because of the computational cost, we have run this simulation for shorter travel times than the other two cases and have used fewer particle pairs (64) per flow realization. As can be seen from figure 5, all three simulations agree well, confirming that the choice $C_1 = 0.1$ is adequate.

The use of a time-step based on the classical correlation time scale $r^{2/3}/\varepsilon^{1/3}$ was also investigated. Here

$$\Delta t = C_4 \min\left(\frac{r^{2/3}}{\epsilon^{1/3}}, \frac{L}{\overline{U}}\right) \tag{11}$$

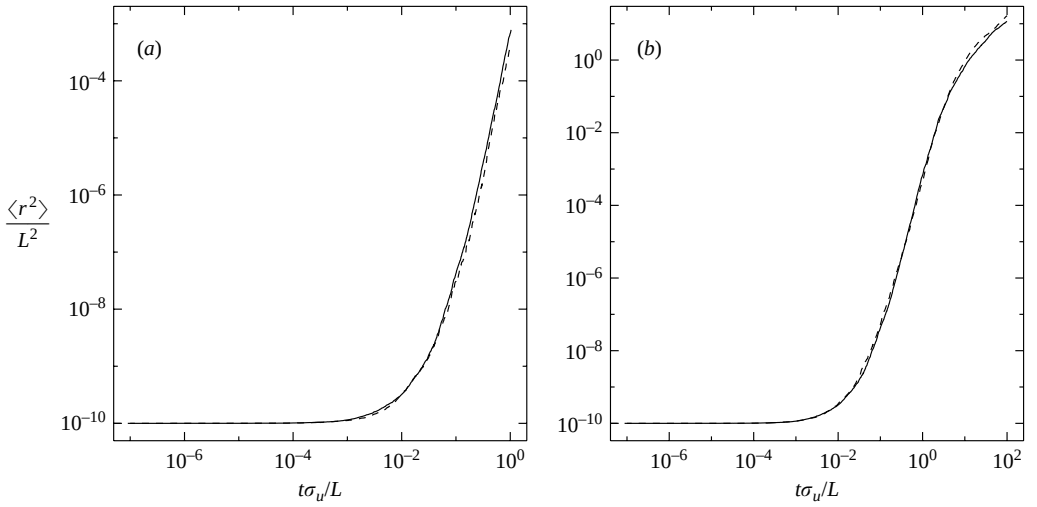


FIGURE 5. Results of time-step sensitivity tests for the case of a strong mean flow. The base case (solid) which uses $C_1 = 0.1$ is compared in (*a*) with a simulation with $\Delta t = 0.1\eta/\overline{U}$ (dashed), and in (*b*) with a simulation with $C_1 = 0.01$ (dashed). Apart from the choice of time-step and, for the expensive simulation with $\Delta t = 0.1\eta/\overline{U}$, the time over which the simulation is run and the number of particle pairs (64) per flow realization, the parameters of these simulations are the same.

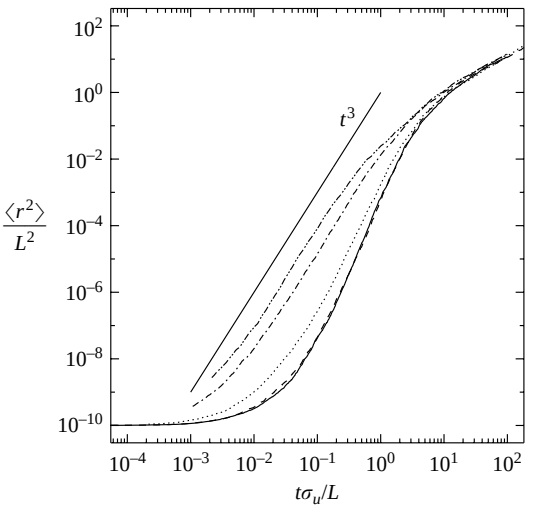


FIGURE 6. Results of simulations performed with the time-step (11). Results are shown for $C_4 = 0.1$ (– · · –), $C_4 = 0.05$ (– · –), $C_4 = 0.01$ (· · ·) and $C_4 = 0.001$ (– – –), and are compared with the base-case simulation (solid). Apart from the choice of time-step, the parameters of these simulations are the same. The straight line is proportional to $t^3$.

which, for an appropriate value of $C_4$, should be small enough for real flows but not for kinematic simulation (for the reasons discussed in § 2). For small $r$, $\Delta t$ will be much larger than the sweeping de-correlation time $r/\overline{U}$. Since the numerical method in effect holds the particle velocities constant over the time $\Delta t$, the effective de-correlation time will be determined by $\Delta t$ and, since $\Delta t$ obeys the classical scaling, we expect $\langle r^2\rangle$ to show the classical $t^3$ behaviour. This is confirmed by the results in figure 6 using (11) with $C_4 = 0.1$. However, by making $C_4$ very small, it is clearly

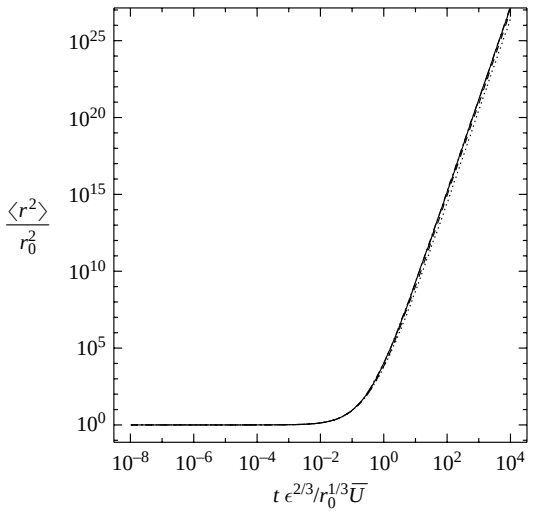


FIGURE 7. Results of time-step sensitivity tests for the random walk simulation. Results are shown for $C_3 = 0.1$ ($\cdots$), $C_3 = 0.01$ ($- - -$), $C_3 = 10^{-3}$ (solid) and $C_3 = 10^{-4}$ ($- \cdot -$). The $C_3 = 10^{-3}$ and $C_3 = 10^{-4}$ results are indistinguishable in the figure.

possible to ensure that the time-step is small enough, and the results obtained using the time-step (4) are recovered when $C_4 = 0.001$. Elliott & Majda (1996) chose a time-step which is of order (11) and so this may explain their observed extensive $t^3$ regime. However, their simulations were two-dimensional and their time-step varied with the relative velocity of the pair which complicates the situation somewhat.

We also conducted tests on the sensitivity of the random walk simulation to the time-step. The random walk simulation shown in figures 3 and 4 was repeated with various values of $C_3$ and the results are shown in figure 7. It shows the mean-square separation converging as $C_3$ decreases and confirms that the choice $C_3 = 10^{-3}$ is adequate.

Our initial attempts to produce the above results used only 120 Fourier modes and were rather noisy. This can be understood as follows. In single-particle dispersion, the Lagrangian integral time scale is proportional to the Lagrangian energy spectral density at zero frequency (see e.g. Pasquill & Smith 1983, p. 23). Any mode with a non-zero frequency will, for large enough travel time, simply cause oscillations and will not cause the particle dispersion to increase. Similar effects can be expected in our simulations, except that here it is the (Eulerian) energy spectral density on the plane $\boldsymbol{k} \cdot \overline{\boldsymbol{U}} = 0$ which is important. This can be understood if we re-write equations (6) and (7) for $K_{ij}$ as

$$\begin{aligned} K_{ij} &= \frac{1}{2} \int_{-\infty}^{\infty} [2R_{ij}(\overline{\boldsymbol{U}}t') - R_{ij}(\overline{\boldsymbol{U}}t' - \boldsymbol{r}) - R_{ij}(\overline{\boldsymbol{U}}t' + \boldsymbol{r})]\, \mathrm{d}t' \\ &= \frac{2\pi}{\overline{U}} \int_{-\infty}^{\infty} \int_{-\infty}^{\infty} (1 - \cos(k_2 r_2 + k_3 r_3)) \Phi_{ij}(0, k_2, k_3)\, \mathrm{d}k_2\, \mathrm{d}k_3 \end{aligned} \tag{12}$$

where $R_{ij}$ is the two-point velocity correlation tensor and $\Phi_{ij}(\boldsymbol{k})$ is the velocity spectrum tensor. Now, in the numerical simulation, $\Phi_{ij}(0, k_2, k_3)$ will almost certainly be zero because of the zero probability of choosing a mode to lie exactly on the plane $k_1 = 0$. However, provided the modes are reasonably densely distributed, it seems likely that the numerical simulation will represent $R_{ij}$ reasonably accurately except in

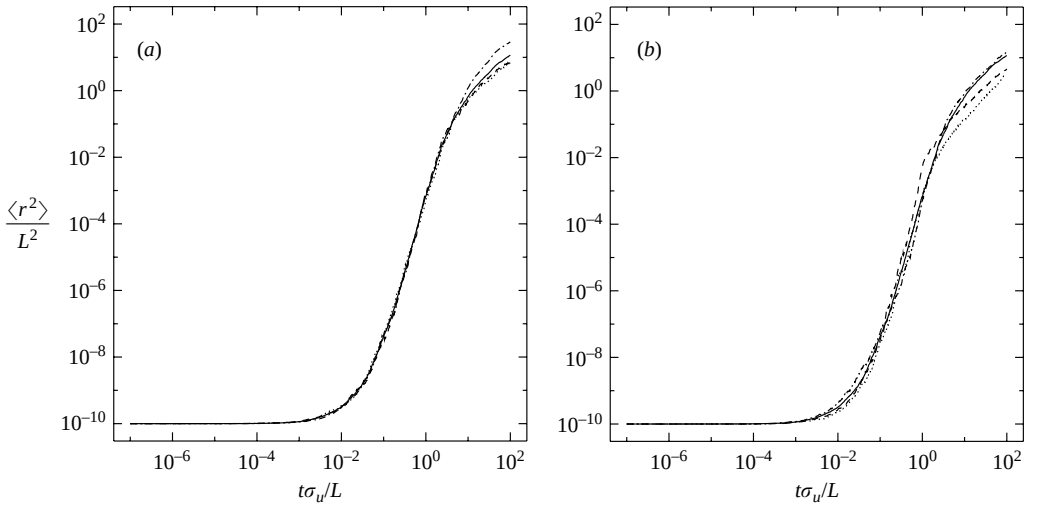


FIGURE 8. Illustration of the variability between realizations and its relation to the number of modes used: (*a*) the base-case result (solid) and three separate realizations with the same parameters (these simulations use 1200 modes); (*b*) the base-case result (solid) and three separate realizations using the same parameters but with 120 modes. In (*b*) we compare with the base-case result (and not with the average of the 120 mode simulations) because that is our best estimate of the correct behaviour for a large number of modes.

the extreme tail. This will lead to the integral for $K_{ij}$ converging to approximately the correct value if integrated over some finite range even though the full integral over $(-\infty, \infty)$ is zero. This will give acceptable results provided the particles have moved on to a significantly different value of the separation before the effect of the tail can come into play. However, if the modes are not sufficiently densely distributed, the results in any one realization may be rather unpredictable and noisy. We expect the integral in (12) to be dominated by values of $|(k_2, k_3)|$ of order $1/|(r_2, r_3)|$, so that eddies with size (in the (2,3)-direction) of order the separation dominate the separation process. As a result, in order to reduce the variability in $K_{ij}(\boldsymbol{r})$ between realizations of the flow, we require enough modes to ensure that there are modes close to the plane $k_1 = 0$ with $|(k_2, k_3)|$ of order $1/|(r_2, r_3)|$. To reduce the variability in the separation statistics between different realizations, this must be true for all relevant separations $r$.

This suggests that, for a small number of modes, the variability in results between different realizations of the flow will be significant and that this variability will remain even if many pairs are followed in each realization. Indeed it seems possible that separation rates could be too low even when averaged over many realizations; if the effective $K$ is small at a particular magnitude of the separation this could act as a blockage to the separation process which is not corrected by $K$ being larger than average at other values of the separation. On the other hand, fluctuations in $K$ could systematically increase $\langle r^2 \rangle$ because, if $K$ is altered by a factor $f$ which is independent of $r$ and has mean unity (e.g. with $f$ varying with location in the flow or between realizations), then $\langle r^2 \rangle$ will be altered by a factor $\langle f^6 \rangle$ which is greater than unity.

Figure 8 shows the sensitivity of the kinematic simulation to the number of modes, with the base case (1200 modes) being compared with simulations with only 120 modes. With 120 modes the results are clearly noisier, although there is little conclusive evidence of $\langle r^2 \rangle$ being systematically larger or smaller. There is a suggestion

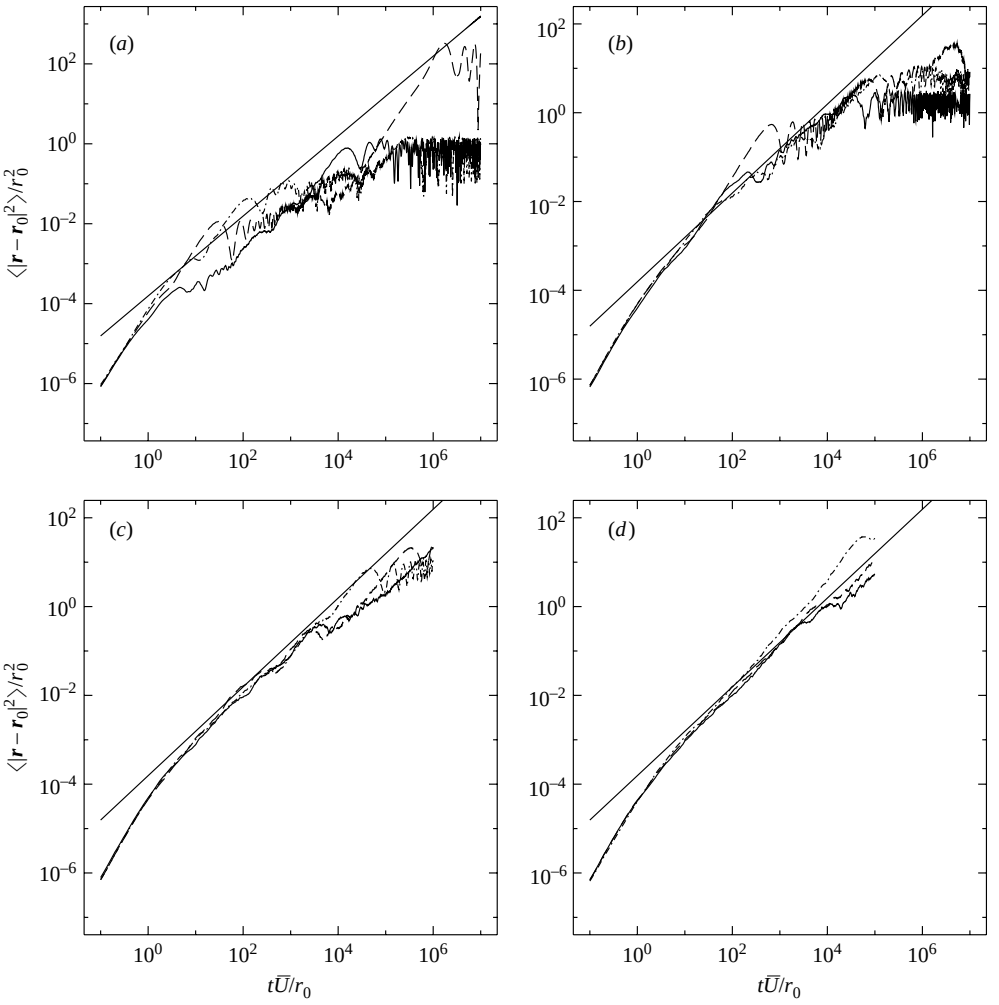


FIGURE 9. The evolution of $\langle|\boldsymbol{r}-\boldsymbol{r}_0|^2\rangle$ for particles moving with the velocity evaluated at the point where the particle would be if it moved only with the mean flow. Each plot shows three realizations, with the results in (*a*), (*b*), (*c*) and (*d*) computed with 12, 120, 1200 and 12000 modes respectively. The time-step is based on (4) but evaluated using the initial separation. All other simulation parameters are as in the base case (apart from the time over which the simulations are run). The straight line is $\langle|\boldsymbol{r}-\boldsymbol{r}_0|^2\rangle = 2\tilde{K}_{ii}(r_0)t$.

of the noise increasing at large times, which is not unexpected if the effect of the noise is cumulative.

The problem with the lack of modes exactly on the plane $k_1 = 0$ can be illustrated more clearly by moving the particles with a velocity evaluated at the point where the particle would be if it moved only with the mean flow. In this case the approximations made in (6) and (7) are exact and, for $t \gg r_0/\overline{U}$, the separation is governed by a diffusion equation with constant eddy diffusivity $K_{ij}(\boldsymbol{r}_0)$. Figure 9 shows the evolution of $\langle|\boldsymbol{r}-\boldsymbol{r}_0|^2\rangle$ for this situation with the number of modes $N$ equal to 12, 120, 1200 and 12000. For small $N$ it clearly shows $\langle|\boldsymbol{r}-\boldsymbol{r}_0|^2\rangle$ levelling off at travel times much greater than $r_0/\overline{U}$ (due to $\Phi_{ij}(0, k_2, k_3)$, and hence $K_{ij}$, being zero) although there is a period after $r_0/\overline{U}$ and before the extreme tail in $R_{ij}$ comes into play where the results

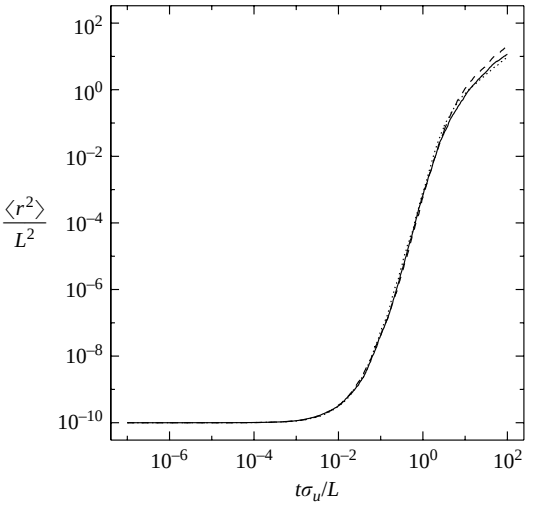


FIGURE 10. Illustration of the effect of unsteadiness. The base case (solid) which has $\lambda = 0$ is compared with simulations with $\lambda = 1$ (dashed) and $\lambda = 5$ (dotted) but which are otherwise identical.

follow roughly $2\tilde{K}_{ii}t$ as given by (10). At large times, the mean-square separation's size and degree of oscillation show significant variability between realizations. This is expected because they depend on the precise values of the wavenumber vectors which occur in the simulation. As $N$ increases the results show less noise and follow $2\tilde{K}_{ii}t$ for longer and with greater accuracy.

Figure 10 compares $\langle r^2 \rangle$ computed with unsteady flow fields for $\lambda = 1$ and 5 with that computed by the steady flow field of the base case. For these order-unity values of $\lambda$ the unsteadiness has little effect on the statistics. This may be understood in terms of the time scale over which the relevant wavenumbers are changing. The separation process is dominated by wavenumbers of order $1/r$ and these wavenumbers change on a time scale $r^{2/3}/(\lambda\varepsilon^{1/3})$. For $\lambda$ of order unity, this is of order the classical time scale $r^{2/3}/\varepsilon^{1/3}$ and is, for small $r$, much larger than the sweeping time scale $\tau(r) \sim r/\overline{U}$. Thus, from the particle pair's perspective, the velocity field is changing much more slowly temporally than spatially and so the unsteadiness has little effect on the statistics.

### 3.2. *Zero mean velocity*

We now consider the case with zero mean velocity and we will restrict our analysis to the inertial-subrange-dominated regime (i.e. we will assume that $r_0 \gg \eta$ and that separations of interest are always much less than $L$). With zero mean flow we expect the sweeping problem will still occur except in those parts of the flow where the velocity is very small. Wherever the sweeping problem is present, we expect the pair-separation eddy diffusivity to be of order $\varepsilon^{2/3}r^{5/3}/u'$ where $u'$ is the local flow speed, and hence we expect the eddy diffusivity to vary with position in the flow according to the size of the local velocity. In the bulk of the flow $u'$ will be of order $\sigma_u$ and so we expect $K$ to be of order $\varepsilon^{2/3}r^{5/3}/\sigma_u$. However the estimate $\varepsilon^{2/3}r^{5/3}/u'$ diverges at small $u'$, and will be regularized by the fact that, for small $u'$, the sweeping problem disappears and this estimate no longer applies. At small $u'$ we expect the classical scaling to apply, with the correlation time $\tau(r)$ being of order $r^{2/3}/\varepsilon^{1/3}$ and $K$ being of order $\varepsilon^{1/3}r^{4/3}$.

On first thoughts it seems plausible that the separation process might be understood by estimating the average value of $K(\boldsymbol{r})$ across the flow. Since the velocity field is Gaussian, the p.d.f. of $u'$ is given by

$$p(u') = \frac{4\pi u'^2}{(2\pi)^{3/2}\sigma_u^3}\exp\left(-\frac{u'^2}{2\sigma_u^2}\right)$$

and $K$ can be estimated as

$$\int_0^\infty \frac{\varepsilon^{2/3}r^{5/3}}{u'}p(u')\,\mathrm{d}u'.$$

Since this converges at $u'=0$, it seems likely that the small-$u'$ behaviour does not play a significant role and there seems no need to consider explicitly the small-$u'$ regions where the sweeping problem is absent. However this is not in fact correct. It turns out that a better approximation is to assume that $u'$ is approximately constant during the dispersion process (at least until the separation becomes of order $L$). Then one can evaluate the mean-square separation conditional on $u'$. If we write this as $\langle r^2\rangle|_{u'}$ then we have $\langle r^2\rangle|_{u'} \sim \varepsilon^4 t^6/u'^6$ in the power-law regime. When averaged over $u'$ this diverges at small $u'$ implying that $\langle r^2\rangle$ cannot be calculated without taking more explicit account of the regions with small $u'$. Note that, in real turbulence, we would not expect regions of small $u'$ to be substantially different from other regions when the latter are viewed in a frame moving with the local flow, and hence we would not expect the small-$u'$ regions to play such a key role.

To account for these small-$u'$ regions we will make the approximation of assuming the dispersion is governed by an eddy diffusivity. This is likely to be accurate in the regions with large $u'$ and strong sweeping, and should also give the correct scaling properties in regions with small $u'$. We also assume the sweeping velocity $u'$ does not change significantly during the evolution; this will be justified below. The effective correlation time scale for the relative velocity at separation $r$ will now depend on $u'$ and be given by

$$\tau(r,u') \sim \min\left(\frac{r}{u'}, \frac{r^{2/3}}{\varepsilon^{1/3}}\right). \tag{13}$$

Here $r/u'$ is the de-correlation time due to sweeping through the eddies at velocity $u'$ and $r^{2/3}/\varepsilon^{1/3}$ is the classical de-correlation time due to advection by eddies of scale $r$ and, if $\lambda \neq 0$, due to evolution of eddies of scale $r$ (note that here, as in most of the rest of the paper, we are assuming that, if $\lambda \neq 0$, then $\lambda$ is of order unity and hence that the evolution time scale is of order $r^{2/3}/\varepsilon^{1/3}$). The overall de-correlation time scale is the smaller of these two scales because it is controlled by whichever of the two processes happens fastest. This leads to an eddy diffusivity given by

$$K(r,u') \sim \min\left(\frac{\varepsilon^{2/3}r^{5/3}}{u'}, \varepsilon^{1/3}r^{4/3}\right).$$

The dividing point between the small- and large-$u'$ forms of $\tau$ and $K$ occurs at $u' \sim \varepsilon^{1/3}r^{1/3}$. We also have that the take-off time at initial separation $r_0$ is determined by $K(r_0)t_{to} \sim r_0^2$ and hence given by

$$t_{to}(r_0,u') \sim \max\left(\frac{r_0^{1/3}u'}{\varepsilon^{2/3}}, \frac{r_0^{2/3}}{\varepsilon^{1/3}}\right).$$

The dependence on $u'$ of the initial correlation time $\tau(r_0,u')$ and the take-off time is shown schematically in figure 11. Four different regimes where we expect different

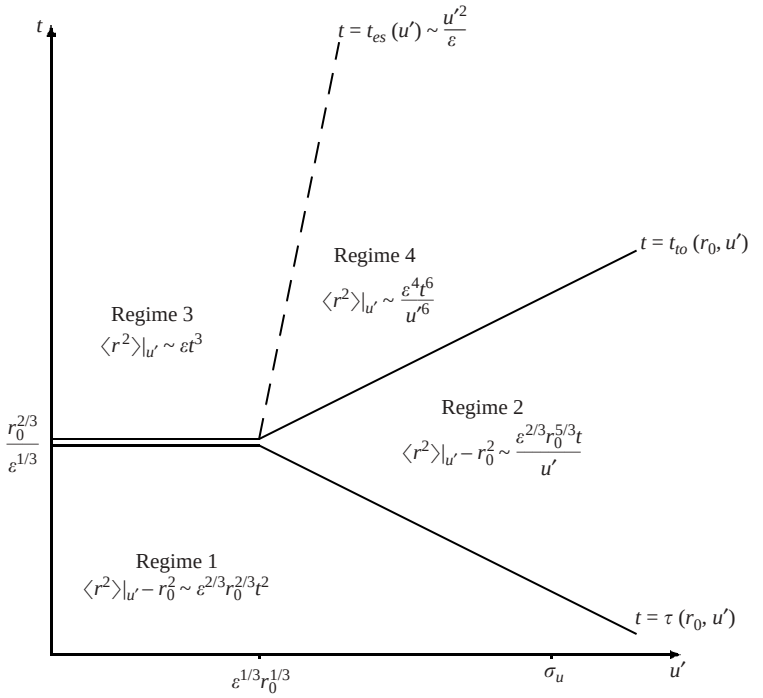


FIGURE 11. A log-log schematic representation of the physics of the zero-mean-flow case. The variation with the sweeping velocity $u'$ of the correlation time $\tau(r_0, u')$ and the take-off time $t_{to}(r_0, u')$ is shown. The four regimes discussed in the text are also shown, including the behaviour of $\langle r^2 \rangle|_{u'}$ in each of the regimes and the position of the dividing line between regimes 3 and 4 which is characterized by the end-of-sweeping time $t_{es}(u')$.

behaviour to occur have been identified in figure 11 and the form of the behaviour noted. In the first regime, the time is less than the correlation time $\tau$ and the correct order of magnitude result can be obtained by approximating particle trajectories by straight lines. This leads to $\langle r^2 \rangle|_{u'} - r_0^2 \sim \varepsilon^{2/3} r_0^{2/3} t^2$. In regime 2, $t$ is greater than $\tau$, but particle pairs have not yet changed their separation substantially. Hence $\langle r^2 \rangle|_{u'} - r_0^2 \sim K(r_0, u')t \sim \varepsilon^{2/3} r_0^{5/3} t/u'$. For travel times larger than the take-off time, we expect

$$\langle r^2 \rangle|_{u'} \sim \varepsilon t^3 \tag{14}$$

in the regime where $\tau$ and $K$ have their classical scalings (regime 3) and

$$\langle r^2 \rangle|_{u'} \sim \varepsilon^4 t^6 / u'^6 \tag{15}$$

in the sweeping dominated regime (regime 4). The classical case should occur when $\tau(r, u') \sim r^{2/3}/\varepsilon^{1/3}$ and the sweeping-dominated case when $\tau(r, u') \sim r/u'$, with, as discussed above, the dividing point at $u' \sim \varepsilon^{1/3} r^{1/3}$. For given $u'$ and $t$, the vast majority of the particles will have a separation $r$ of order $\langle r^2 \rangle|_{u'}^{1/2}$. Hence, by using either (14) or (15) and the relation $u' \sim \varepsilon^{1/3} r^{1/3}$, we calculate that the dividing line between regimes 3 and 4 is given by $u' \sim (\varepsilon t)^{1/2}$. Note that the two regimes match appropriately on this line. We can also regard this dividing line as defining the 'end-of-sweeping time' $t_{es} \sim u'^2/\varepsilon$ at which the sweeping-dominated regime comes to an end. At this time, the typical relative velocity of the particle pairs which start in the

sweeping regime is given by $\Delta u \sim \varepsilon^{1/3} r^{1/3} \sim \varepsilon^{1/3} \langle r^2 \rangle^{1/6} \sim u'$. This is consistent with the fact that the problem cannot be dominated by sweeping with velocity $u'$ when the relative velocity of the particles is as large as $u'$. At time $t_{es}$, and indeed throughout regime 3, the correlation time $\tau$ is of order the travel time.

We can now return to consider whether we are justified in ignoring changes in $u'$. For pairs that start in the classical regime, the typical change in a particle's velocity over time $t$ will be of order $(\varepsilon t)^{1/2}$ (Monin & Yaglom 1975, p. 359). This change in $u'$ will not move the pair out of the classical regime and so the above analysis (which ignores the change in $u'$) will give results with the correct order of magnitude. For pairs that start in the sweeping regime, the typical change in a particle's velocity over time $t$ is dominated by the sweeping process and will be of order $(\varepsilon u' t)^{1/3}$. Until the time becomes of order $t_{es}$ and the sweeping regime comes to an end, the change of order $(\varepsilon u' t)^{1/3}$ in $u'$ is much less than $u'$ and so can be ignored.

As an aside we note that the velocity change of order $(\varepsilon u' t)^{1/3}$ which occurs in the sweeping regime is not what would be expected in real turbulence and is a manifestation of the effect of the sweeping problem on one-particle statistics – see Malik (1991) and Fung *et al.* (1992). In real turbulence we expect the Lagrangian structure function to remain proportional to $\varepsilon t$ with the velocity change of order $(\varepsilon t)^{1/2}$. We should also comment that the arguments above assume $\lambda$ no larger than order unity. For very large $\lambda$ we do expect the Lagrangian structure function in the kinematic simulations to be proportional to $t$ but with a coefficient proportional to $\lambda\varepsilon$. This is a result of unsteadiness rather than sweeping dominating the change in velocity, and can be derived by integrating $E(k)$ over the range of wavenumbers which are expected to have changed significantly over time $t$, i.e. wavenumbers which are greater than the wavenumber at which $\omega(k)t \sim 1$. Although in this situation the Lagrangian structure function has the correct power-law exponent, the coefficient $\lambda\varepsilon$ is too large and so we do not regard making $\lambda$ large as a satisfactory way to rectify the sweeping problem. For $\lambda \gg 1$ but not so large that the unsteadiness time scale $1/\omega$ is smaller than the sweeping time scale $1/\sigma_u k$ for even the smallest modes, a Lagrangian structure function regime proportional to $t^{2/3}$ followed by one proportional to $t$ seems likely. See Khan & Vassilicos (2004) for some discussion and simulations related to these ideas.

When averaged over all $u'$, the mean-square separation is given by

$$\langle r^2 \rangle = \int_0^\infty \langle r^2 \rangle|_{u'}\, p(u')\, \mathrm{d}u'. \tag{16}$$

By combining this with the information in figure 11 we can derive expressions for the evolution of $\langle r^2 \rangle$. Here we only consider travel times much larger than $t_{to}(r_0, \sigma_u) \sim r_0^{1/3}\sigma_u/\varepsilon^{2/3}$ in detail, but other regimes can be treated similarly. For $t \gg t_{to}(r_0, \sigma_u)$, (16) can be divided into three contributions from the regimes 3, 4 and 2 in figure 11. This yields

$$\langle r^2 \rangle \sim \int_0^{\sqrt{\varepsilon t}} \varepsilon t^3\, p(u')\, \mathrm{d}u' + \int_{\sqrt{\varepsilon t}}^{t\varepsilon^{2/3}/r_0^{1/3}} \frac{\varepsilon^4 t^6}{u'^6}\, p(u')\, \mathrm{d}u' + \int_{t\varepsilon^{2/3}/r_0^{1/3}}^\infty \left( r_0^2 + \frac{\varepsilon^{2/3} r_0^{5/3} t}{u'} \right) p(u')\, \mathrm{d}u'.$$

The first and second terms both make a contribution of order $\varepsilon^{5/2} t^{9/2}/\sigma_u^3$ while the last term is negligible in comparison. Hence

$$\langle r^2 \rangle \sim \frac{\varepsilon^{5/2} t^{9/2}}{\sigma_u^3}. \tag{17}$$

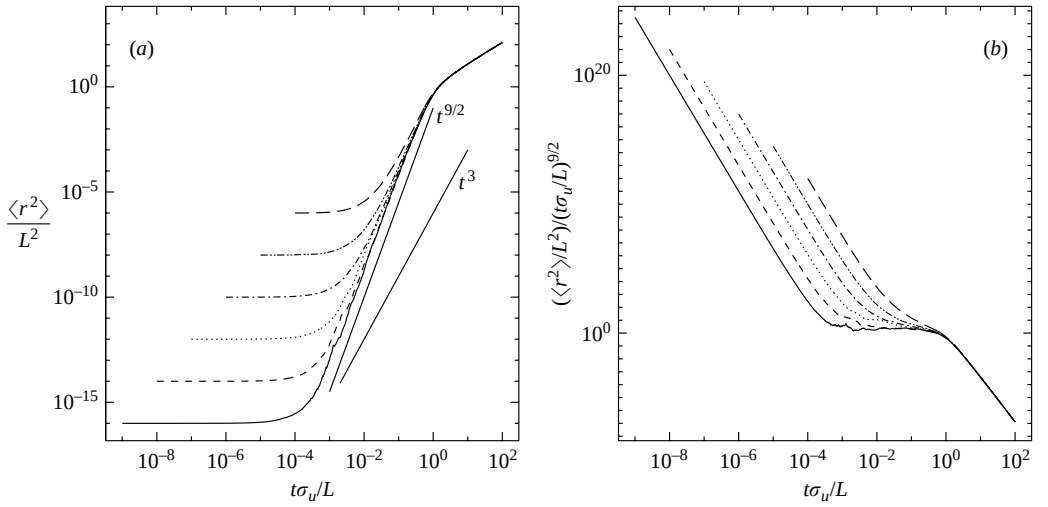


FIGURE 12. The evolution of $\langle r^2\rangle$ for $\overline{U}=0$, $\lambda=0$, 125 particle pairs per realization and 20 realizations of the flow in each simulation. (*a*) Results for $r_0/L=10^{-8}$, $10^{-7}$, $10^{-6}$, $10^{-5}$, $10^{-4}$ and $10^{-3}$ (bottom to top) with $\eta/L=10^{-8}$ and $N=1600$. The straight lines are proportional to $t^3$ and $t^{9/2}$. (*b*) The evolution of $\langle r^2\rangle/t^{9/2}$ for the same simulations.

Figure 12(*a*) shows the evolution of $\langle r^2\rangle$ as computed using the kinematic simulation technique for the case of zero mean flow. A range of initial separations $r_0$ are used, namely

$$r_0/L = 10^{-8}, 10^{-7}, 10^{-6}, 10^{-5}, 10^{-4} \text{ and } 10^{-3}$$

with $\eta/L=10^{-8}$ and 1600 modes. These simulations are steady flows (i.e. $\lambda=0$) with 125 particle pairs per realization and 20 realizations of the flow in each simulation. Examination of figure 12(*a*) shows that $\langle r^2\rangle$ is constant at small times but then, at least for the smaller values of $r_0$, grows like $t^{9/2}$ as predicted. At large times $\langle r^2\rangle$ grows linearly. The results are consistent with the expectation that, for small $r_0/L$ and $\eta/L$ (with $r_0 \ll \eta$), the values of $r_0$ and $\eta$ are forgotten at large times and that this happens long before the linear regime is reached. Figure 12(*b*) shows the evolution of $\langle r^2\rangle/t^{9/2}$. For the smaller values of $r_0/L$, this shows convincing evidence of a $t^{9/2}$ regime at intermediate travel times with the length of the regime increasing as $r_0/L$ decreases. We note that the size of the interval in which this behaviour is observed is longer than the corresponding intermediate time interval for the case of non-zero mean velocity in § 3.1 (where the mean-square separation grows like $t^6$). This is perhaps to be expected because the lower power means that a larger fractional change in time is needed for $\langle r^2\rangle$ to grow from $\eta^2$ to $L^2$.

As for the case with a strong mean flow, we have investigated the sensitivity of the results to the time-step. Figure 13 compares the case with $r_0/L=10^{-7}$ and $\eta/L=10^{-8}$ from figure 12 (for which $C_1=0.1$) with two other simulations using the same values of $r_0/L$ and $\eta/L$, one with a fixed-time-step of $0.1\eta/\sigma_u$ and one with an adaptive time-step given by (4) with $C_1=0.01$. Because of the computational cost, we have run the fixed-time-step simulation for shorter travel times than the other two cases and have used fewer particle pairs (64) per flow realization and fewer flow realizations (5). There is good agreement between the simulations, supporting the adequacy of our choice of time-step.

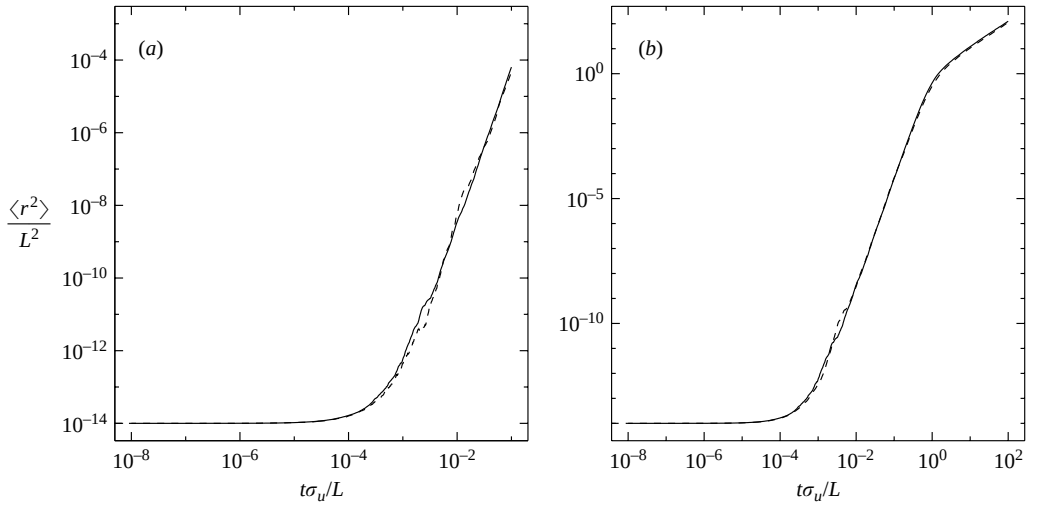


FIGURE 13. Results of time-step sensitivity tests for the case of no mean flow. The simulation from figure 12 with $r_0/L = 10^{-7}$ and $\eta/L = 10^{-8}$ (solid) (this simulation uses $C_1 = 0.1$) is compared in (*a*) with a simulation with $\Delta t = 0.1\eta/\sigma_u$ (dashed), and in (*b*) with a simulation with $C_1 = 0.01$ (dashed). Apart from the choice of time-step and, for the expensive simulation with $\Delta t = 0.1\eta/\sigma_u$, the time over which the simulation is run, the number of particle pairs (64) per flow realization and the number of flow realizations (5), the parameters of these simulations are the same.

As noted above, it is possible to analyse the growth of $\langle r^2\rangle$ for other regimes (in the inertial subrange). The result is that

$$\langle r^2\rangle - r_0^2 \sim \varepsilon^{2/3} r_0^{2/3} t^2$$

for $t \ll r_0/\sigma_u$ and

$$\langle r^2\rangle - r_0^2 \sim A\frac{\varepsilon^{2/3} r_0^{5/3} t}{\sigma_u} + B\frac{\varepsilon^{5/2} t^{9/2}}{\sigma_u^3} \tag{18}$$

for $t \gg r_0/\sigma_u$, with the latter case encompassing the regime considered in (17). To explain the meaning of this it is necessary to clarify our use of the '$\sim$' symbol. We have used it in two senses, namely to indicate the rough order of magnitude of a quantity and to indicate proportionality or asymptotic proportionality. For example, we use '$\sim$' in equation (13) to indicate the order of magnitude of $\tau$, but there is no intention to indicate direct proportionality with a kink in $\tau$ at the transition between $r/u'$ and $r^{2/3}/\varepsilon^{1/3}$. However, we also intend to indicate asymptotic proportionality away from the transition, with $\tau$ asymptotically proportional to $r/u'$ for $u' \gg \varepsilon^{1/3} r^{1/3}$. We have not been very precise on such matters because the meaning is, we hope, clear from the context. It is necessary to be more precise however to explain (18). Here we have in mind asymptotic proportionality (or equivalently, since $A$ and $B$ are not given values, asymptotic equality). In particular, we expect the expression given for $t \gg r_0/\sigma_u$ to be valid (with the same values for $A$ and $B$) throughout the transition between the two regimes where one or other of the two terms dominates. The reason for this is that the two terms arise from regions of the flow with very different $u'$ values and these two contributions will continue to evolve in their own way, oblivious to the presence of the other contribution.

In fact we can evaluate the first term on the right-hand side of (18) quantitatively. This term arises from regime 2 and, for fixed $u'$, the contribution is given by (10) with

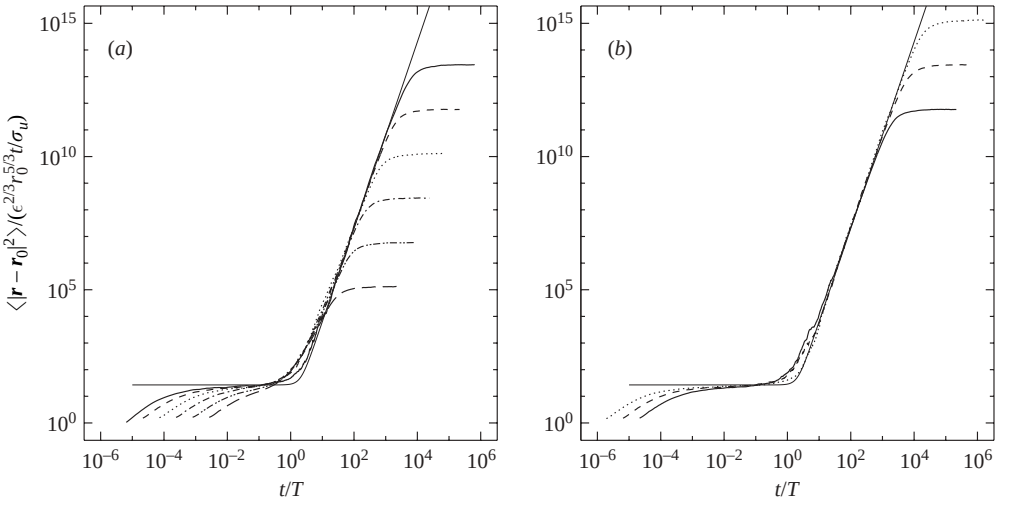


FIGURE 14. The evolution of $\langle|\boldsymbol{r}-\boldsymbol{r}_0|^2\rangle$ for the case of no mean flow. (*a*) The same cases as in figure 12. (*b*) The $r_0/L=10^{-7}$, $\eta/L=10^{-8}$ case from figure 12 (solid) together with cases with (i) $r_0/L=10^{-8}$, $\eta/L=10^{-9}$ and $N=1800$ (dashed), and (ii) $r_0/L=10^{-9}$, $\eta/L=10^{-10}$ and $N=2000$ (dotted), but which are otherwise identical to the figure 12 cases. In both plots the thin solid line is given by the right-hand side of (20) with $b$ chosen to be 2 (for best visual fit).

$\overline{U}$ replaced by $u'$. Averaging this over $u'$ yields

$$\langle r^2\rangle - r_0^2 \sim \frac{27}{20}\pi(2\pi)^{1/6}\frac{\Gamma(1/6)\Gamma(5/6)}{\Gamma(2/3)}\frac{\epsilon^{2/3}r_0^{5/3}t}{\sigma_u} + b\frac{\epsilon^{5/2}t^{9/2}}{\sigma_u^3} \tag{19}$$

for some constant $b$, where we have expressed the result in terms of $\epsilon \equiv \sigma_u^3/L$ to avoid the need to assume a value for the Kolmogorov constant. Here of course we are interpreting '$\sim$' as meaning 'asymptotically equal to'.

To test this idea note that (19) can be written as

$$\frac{\langle r^2\rangle - r_0^2}{\epsilon^{2/3}r_0^{5/3}t/\sigma_u} \sim \frac{9}{20}\pi(2\pi)^{1/6}\frac{\Gamma(1/6)\Gamma(5/6)\Gamma(1/3)}{\Gamma(2/3)\Gamma(4/3)} + b\left(\frac{t}{T}\right)^{7/2} \tag{20}$$

where $T$, a time of order the transition time between the two terms on the right-hand side of (19), is given by

$$T = \frac{r_0^{10/21}\sigma_u^{4/7}}{\epsilon^{11/21}} = \left(\frac{r_0^{2/3}}{\epsilon^{1/3}}\right)^{3/7}\left(\frac{r_0^{1/3}\sigma_u}{\epsilon^{2/3}}\right)^{4/7} \sim \tau(r_0,0)^{3/7}\,t_{to}(r_0,\sigma_u)^{4/7}.$$

In figure 14 we show the simulation results scaled as in (20). Figure 14(*a*) shows the cases that we considered in figure 12. The majority of cases do not follow (20) closely throughout the transition region. The case with the largest $L/r_0$ is closer than the others, but this case has $r_0/\eta=1$ and so the value of $\eta$ might be influencing the results. To investigate this further we did two more simulations with $r_0/L$ equal to $10^{-8}$ and $10^{-9}$ with $r_0/\eta$ fixed at 10. The results are plotted in figure 14(*b*) together with the $r_0/L=10^{-7}$, $r_0/\eta=10$ simulation from figure 14(*a*). This shows more convincing evidence that (20) is correct asymptotically. Because $\tau(r_0,0)$, $T$ and $t_{to}(r_0,\sigma_u)$ all need to be widely separated to see this behaviour it is not surprising that $L/r_0$ needs to be extremely large.

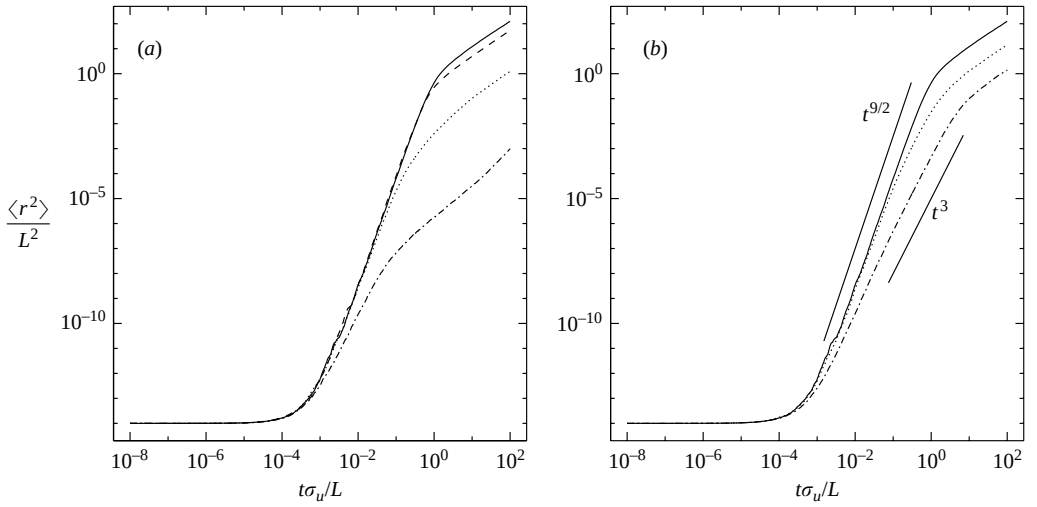


FIGURE 15. Illustration of the effect of unsteadiness for the case of no mean flow. (*a*) The simulation from figure 12 with $r_0/L = 10^{-7}$ and $\eta/L = 10^{-8}$ (solid) (this simulation has $\lambda = 0$) is compared with simulations with $\lambda = 1$ (– – –), $\lambda = 5$ (· · ·) and $\lambda = 25$ (– · –). (*b*) The simulations with $\lambda = 0$, 5 and 25 are repeated, but here the $\omega_n$ values are randomized uniformly between zero and twice the value given by (3). Apart from the values of $\omega_n$ and the fact that the expensive simulation with $\lambda = 25$ and non-random $\omega_n$ uses only 5 realizations, the parameters of these simulations are the same. In (*b*) the straight lines are proportional to $t^3$ and $t^{9/2}$.

Figure 15 shows some investigations of the effect of unsteadiness ($\lambda$) for zero mean flow. We expect the unsteadiness due to $\lambda$ to impose an additional limiting value on the time scale, with (13) being replaced by

$$\tau(r, u') \sim \min\left(\frac{r}{u'}, \frac{r^{2/3}}{\varepsilon^{1/3}}, \frac{r^{2/3}}{\lambda\varepsilon^{1/3}}\right).$$

This will alter the results in regime 3 and will tend to move the dividing line between regimes 3 and 4 to the right. Hence, unlike the strong mean flow case, we expect $\lambda$ to have a significant impact on the results, and this is confirmed in figure 15(*a*). It is possible to repeat the analysis associated with figure 11 for the case of non-zero $\lambda$. This predicts that, as $\lambda$ becomes large, the coefficient of $t^{9/2}$ will decrease with a $t^3$ regime emerging after the $t^{9/2}$ regime. The growth in the $t^3$ regime is predicted to become slower as $\lambda$ increases, being of order $\varepsilon(t/\lambda)^3$. For large enough $\lambda$, the $t^{9/2}$ regime is predicted to disappear completely. However this picture is not seen in the simulations in figure 15(*a*); in particular there is little sign of a $t^3$ regime emerging after a $t^{9/2}$ regime and there is a transition to something like linear growth which, for large $\lambda$, occurs when the mean-square separation is still much less than $L$. It seems possible that this is due to the somewhat singular nature of our choice of the $\omega_n$. This choice leads to no variation close to zero frequency and hence a zero Eulerian integral time scale with negative loops in the Eulerian time correlation function. Arguments such as that sketched above based on the order of magnitude of time scales are likely to fail when correlation functions have substantial negative loops and cannot be described adequately by a single time scale, although its not completely clear that this will be the case here because it is the Lagrangian, not Eulerian, statistics which are crucial for the dispersion. To test this we conducted some simulations in which the $\omega_n$ were chosen with mean value given by (3), but randomized uniformly between zero

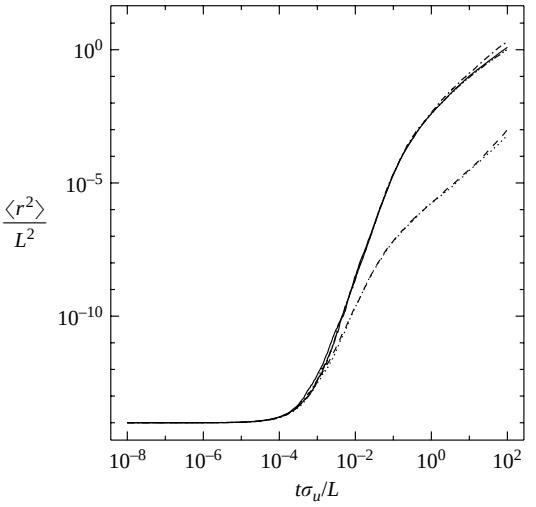


FIGURE 16. Results of time-step sensitivity tests for unsteady cases with no mean flow. The simulations from figure 15(*a*) with $\lambda = 5$ (solid) and $\lambda = 25$ (– – –) (these simulations use $C_2 = 0.01$) are compared with simulations with (i) $\lambda = 5$ and $C_2 = 0.05$ (–·–), (ii) $\lambda = 5$ and $C_2 = 0.001$ (–···–), and (iii) $\lambda = 25$ and $C_2 = 0.005$ (···). The latter three simulations all use only 5 realizations. Apart from the values of $\lambda$ and $C_2$ and the number of realizations, the parameters of these simulations are the same.

and twice the mean. The results, shown in figure 15(*b*), are much more in accordance with our analysis and show that results can be sensitive to the precise way the $\omega_n$ values are chosen. As in the case of the one-particle Lagrangian structure function discussed above, we do not regard making $\lambda$ large as a satisfactory way to rectify the sweeping problem. Although the $t^3$ behaviour is restored for large $\lambda$, we argue that the coefficient, being of order $\varepsilon/\lambda^3$, is too small.

Figure 16 shows the sensitivity to the time-step constant $C_2$ for two of the cases in figure 15(*a*). This shows that $C_2 = 0.01$ appears to be adequately small. It was on the basis of these results that we decided to use $C_2 = 0.01$ in the simulations presented in figures 10 and 15.

It is interesting to speculate on the way the $t^6$ and $t^{9/2}$ behaviours found for large and zero mean flow are related. When there is a mean flow, there will still be a possibility of some particles being in a region of zero velocity, although the fraction of particles involved decreases very rapidly as $\overline{U}/\sigma_u$ increases. If $r_0/L$ is very small (but still with $r_0 \geqslant \eta$), these particles will achieve much larger separations than the majority, and so may still make a significant impact. It therefore seems likely that $t^6$ behaviour occurs as $\overline{U}/\sigma_u \to \infty$ for fixed $r_0/L$ and $t^{9/2}$ behaviour occurs as $r_0/L \to 0$ for fixed $\overline{U}/\sigma_u$. The $t^{9/2}$ regime is likely to be followed by a $t^6$ regime if $\overline{U}/\sigma_u$ is substantially greater than 1. However even for $\overline{U}/\sigma_u = 10$, $r_0/L$ will need to be extraordinarily small to see $t^{9/2}$ and the inertial subrange will need to be extraordinarily long.

## 4. Discussion

We have investigated the separation of pairs of particles in kinematic simulation, with particular attention paid to the problems caused by the lack of sweeping of the small scales by the large scales. We have argued and shown numerically that, in the inertial subrange, the mean-square separation in kinematic simulation grows as $t^6$ in the presence of a strong mean velocity and as $t^{9/2}$ for the case of no mean flow.

This conflicts with the expectation of a Richardson $t^3$ law in real turbulence. It seems plausible that previous $t^3$ results obtained with kinematic simulation are a result either of the asymptotic form not being reached (but with the results following $t^3$ approximately over a short range), or of issues connected with the size of the time-step (see discussion above in connection with figure 6). Support for the possibility that the $t^3$ results are not asymptotic can be found in figures 1 and 12. These show approximate $t^3$ behaviour over a limited range at low $L/r_0$ with the power increasing towards 6 and 9/2 respectively as $L/r_0$ increases. The results of Kurbanmuradov *et al.* (1997), who found a power law intermediate between $t^3$ and $t^{9/2}$, also support this. As a result there seems little reason to prefer the very small values of $G_\Delta$ obtained from such simulations to the values obtained from other models (see discussion in Fung *et al.* 1992). Of course the values of $L/\eta$ in our simulations are very large – comparable to or larger than values in the atmospheric boundary layer – and it is appropriate to ask whether these results are relevant to flows with lower Reynolds numbers. It is hard to make deductions here with confidence, but we believe that, because the asymptotic behaviour does not follow the Richardson scaling, there is little reason to believe that any approximate Richardson behaviour seen over a limited range of scales is a physically realistic representation of the true Richardson law. This also has implications for the application of kinematic simulation to concentration fluctuation problems, the latter being intimately connected with the pair separation problem.

In the above we have considered only $\langle r^2 \rangle$, mainly because calculating other quantities of interest such as the p.d.f. or higher moments of $\boldsymbol{r}$ would require following many more particles and so increase the computational cost. However a few comments are appropriate. Consider first the case with a strong mean flow. If we ignore the tensorial character of $K$ and its dependence on the direction of $\boldsymbol{r}$, then we have $K \sim r^{5/3}$ and the solution of the diffusion equation in the self-similar regime has shape $\exp(-r^{1/3})$. This is much more peaked than the classical Richardson shape $\exp(-r^{2/3})$ corresponding to $K \sim r^{4/3}$. The effect of the tensorial character of $K$ and its dependence on the direction of $\boldsymbol{r}$ is not clear, but this might increase the kurtosis further. This is because $K$ is zero for $\boldsymbol{r}$ aligned with the mean flow $\boldsymbol{U}$ and so pairs whose separation is closely aligned to $\boldsymbol{U}$ will separate more slowly than the rest. For the case of no mean flow there is an additional factor which will tend to increase the kurtosis, namely the fact that the pairs with very different sweeping velocities $u'$ separate at very different rates. The fact that regime 3 in figure 11 makes a contribution to $\langle r^2 \rangle$ of the same order as the total $\langle r^2 \rangle$ despite containing only a small fraction of the particle pairs indicates that a large kurtosis is expected. The larger kurtosis should lead to more noise in $\langle r^2 \rangle$ and some suggestion of this can be found by comparing figure 12 with figures 1 and 2. This is despite the fact that figure 12 uses 4 times as many realizations (of course it was at least partly in order to reduce the noise that we used more realizations in figure 12).

The above suggests that kinematic simulation should in general give too large a kurtosis. However in fact the kurtosis in kinematic simulation agrees well with direct numerical simulations (DNS) (Malik & Vassilicos 1999). This apparent contradiction can be resolved if the large kurtosis in DNS is, as argued by Borgas & Yeung (2004), a consequence of the non-Gaussianity of the two-point (one-time) relative velocity p.d.f., something which is not allowed for within kinematic simulation. Of course the DNS studies (Yeung 1994; Yeung & Borgas 2004) and the work of Borgas & Yeung (2004) are all at low Reynolds numbers and involve the dissipation range. This is not a situation considered in any detail above and so our conclusions here must be regarded as tentative.

The sweeping problem and the idea of an eddy diffusivity varying like $r^{5/3}$ were also considered by Holzer & Siggia (1994). They were not considering pair dispersion per se but the evolution of a passive scalar field. Despite the sweeping problem, they found a scalar inertial–convective subrange which was close to the correct $k^{-5/3}$ scaling. This might be due to the limited range of scales in the simulation (which will reduce the sweeping problem) but it also seems possible that it is due to the simulation being two-dimensional. In a steady two-dimensional flow the streamline topology imposes strong constraints on mixing and so any unsteadiness (Holzer & Siggia's flow was unsteady) is likely to have a stronger effect than in three dimensions and may prevent the sweeping issue from dominating results. This also suggests that some of our results on pair dispersion in kinematic simulation may not carry over to the two-dimensional case. It would be of interest to test this with some two-dimensional simulations.

Although these results raise questions about the applicability of the kinematic simulation approach to the specific problem of pair separation in the three-dimensional inertial subrange, we would emphasize that kinematic simulation remains a valuable tool for many aspects of turbulent dispersion. For example the sweeping problem disappears in the white noise limit, a limit which seems to preserve many dispersive properties of real turbulence. There are also many problems where the sweeping issue is not important, such as flows with a limited range of scales, possibly two-dimensional flows (see the above discussion in connection with Holzer & Siggia's 1994 results), and one-particle dispersion problems. For one-particle problems, it is possible to consider the effect of plane boundaries (Turfus & Hunt 1987) or stable stratification (Nicolleau & Vassilicos 2000) in effect via a rapid distortion calculation, and more complex flows may also be possible. In addition, it provides useful cases for testing ideas on the 'generalized dispersion problem' (i.e. given a set of flow statistics, what are the dispersion statistics), even if the flows addressed have some properties which are not realistic for real turbulence. In this context we note that the study presented above does help to answer questions about the value of the 'statistical approach' and the use of the 'eddy-diffusivity' concept for relative dispersion (although it may be that these concepts are better for kinematic simulation than for real turbulence). Here we have in mind the contrast and debate between the 'statistical' and the 'structural' views (see Lumley 1990) and believe that both approaches are important in developing our understanding of turbulence. Finally we note that the kinematic simulation results with a strong mean flow may well be relevant to the turbulent spread of rapidly falling particles (although that problem is usually complicated by the effects of particle inertia). This is because the fall speed will lead to particles cutting through the eddies in the same way as in the kinematic simulations.

The authors would like to thank Christos Vassilicos and Franck Nicolleau for the loan of a kinematic simulation code which was used to perform some preliminary studies for this paper.

## REFERENCES

Batchelor, G. K. 1952 Diffusion in a field of homogeneous turbulence. II. The relative motion of particles. *Proc. Camb. Phil. Soc.* **48**, 345–362.

Borgas, M. S. & Yeung, P. K. 2004 Relative dispersion in isotropic turbulence: Part 2. A new stochastic model with Reynolds number dependence. *J. Fluid Mech.* **503**, 125–160.

Durbin, P. A. 1980 A stochastic model of two-particle dispersion and concentration fluctuations in homogeneous turbulence. *J. Fluid Mech.* **100**, 279–302.

Elliott, F. W. & Majda, A. J. 1996 Pair dispersion over an inertial range spanning many decades. *Phys. Fluids* **8**, 1052–1060.

Eyink, G. L. & Xin, J. 2000 Self-similar decay in the Kraichnan model of a passive scalar. *J. Statist. Phys.* **100**, 679–741.

Flohr, P. & Vassilicos, J. C. 2000 A scalar subgrid model with flow structure for large-eddy simulations of scalar variances. *J. Fluid Mech.* **407**, 315–349.

Fung, J. C. H., Hunt, J. C. R., Malik, N. A. & Perkins, R. J. 1992 Kinematic simulation of homogeneous turbulence by unsteady random Fourier modes. *J. Fluid Mech.* **236**, 281–318.

Fung, J. C. H. & Vassilicos, J. C. 1998 Two-particle dispersion in turbulent-like flows. *Phys. Rev.* E **57**, 1677–1690.

Holzer, M. & Siggia, E. D. 1994 Turbulent mixing of a passive scalar. *Phys. Fluids* **6**, 1820–1837.

Khan, M. A. L. & Vassilicos, J. C. 2004 A new Eulerian-Lagrangian length-scale in turbulent flows. *Phys. Fluids* **16**, 216–218.

Kraichnan, R. H. 1959 The structure of isotropic turbulence at very high Reynolds numbers. *J. Fluid Mech.* **5**, 497–543.

Kraichnan, R. H. 1966 Dispersion of particle pairs in homogeneous turbulence. *Phys. Fluids* **9**, 1937–1943.

Kraichnan, R. H. 1968 Small-scale structure of a scalar field convected by turbulence. *Phys. Fluids* **11**, 945–953.

Kraichnan, R. H. 1994 Anomalous scaling of a randomly advected passive scalar. *Phys. Rev. Lett.* **72**, 1016–1019.

Kurbanmuradov, O. 1995 Convergence of numerical models for the Gaussian fields. *Russ. J. Numer. Anal. Math. Modelling* **10**, 311–323.

Kurbanmuradov, O., Sabelfeld, K. & Koluhin, D. 1997 Stochastic Lagrangian models for two-particle motion in turbulent flows. Numerical results. *Monte Carlo Meth. Appl.* **3**, 199–223.

Lumley, J. L. (Ed.) 1990 *Whither Turbulence? Turbulence at the Crossroads*. Springer.

Malik, N. A. 1991 Studies in turbulent dispersion using kinematic simulation. PhD thesis, University of Cambridge.

Malik, N. A. & Vassilicos, J. C. 1999 A Lagrangian model for turbulent dispersion with turbulent-like flow structure: comparison with direct numerical simulation for two-particle statistics. *Phys. Fluids* **11**, 1572–1580.

Monin, A. S. & Yaglom, A. M. 1975 *Statistical Fluid Mechanics*, vol. 2. The MIT Press.

Nicolleau, F. & Vassilicos, J. C. 2000 Turbulent diffusion in stably stratified non-decaying turbulence. *J. Fluid Mech.* **410**, 123–146.

Ott, S. & Mann, J. 2000 An experimental investigation of the relative diffusion of particle pairs in three-dimensional turbulent flow. *J. Fluid Mech.* **422**, 207–223.

Pasquill, F. & Smith, F. B. 1983 *Atmospheric Diffusion*, 3rd edn. Ellis Horwood, Chichester.

Richardson, L. F. 1926 Atmospheric diffusion shown on a distance-neighbour graph. *Proc. Roy. Soc. Lond.* A **110**, 709–737.

Sabelfeld, K. K. & Kurbanmuradov, O. A. 1990 Numerical statistical model of classical incompressible isotropic turbulence. *Sov. J. Numer. Anal. Math. Modelling* **5**, 251–263.

Taylor, G. I. 1921 Diffusion by continuous movements. *Proc. Lond. Math. Soc.* 2, **20**, 196–212.

Tennekes, H. 1975 Eulerian and Lagrangian time microscales in isotropic turbulence. *J. Fluid Mech.* **67**, 561–567.

Thomson, D. J. 1990 A stochastic model for the motion of particle pairs in isotropic high Reynolds number turbulence, and its application to the problem of concentration variance. *J. Fluid Mech.* **210**, 113–153.

Thomson, D. J. & Devenish, B. J. 2003 Particle pair separation in kinematic simulations. *Met Office Turbulence and Diffusion Note* 289, available from the UK National Meteorological Library.

Turfus, C. & Hunt, J. C. R. 1987 A stochastic analysis of the displacements of fluid elements in inhomogeneous turbulence using Kraichnan's method of random modes. In *Advances in Turbulence* (ed. G. Comte-Bellot & J. Mathieu). Springer.

Yeung, P. K. 1994 Direct numerical simulation of two-particle relative diffusion in isotropic turbulence. *Phys. Fluids* **6**, 3416–3428.

Yeung, P. K. & Borgas, M. S. 2004 Relative dispersion in isotropic turbulence: Part 1. Direct numerical simulations and Reynolds number dependence. *J. Fluid Mech.* **503**, 93–124.